IEEE Access
Multidisciplinary | Rapid Review | Open Access Journal

Received September 21, 2019, accepted October 6, 2019, date of publication October 11, 2019, date of current version October 24, 2019.

Digital Object Identifier 10.1109/ACCESS.2019.2947057

Directive Low-Band UWB Antenna for In-body Medical Communications

CHAÏMAÂ KISSI[1], MARIELLA SÄRESTÖNIEMI[2], TIMO KUMPUNIEMI[2], MARKO SONKKI[2], SAMI MYLLYMÄKI[3], MOHAMED NABIL SRIFI[1], AND CARLOS POMALAZA-RAEZ[4], (Senior Member, IEEE)

[1]Electronics and Telecommunication Systems Research Group, National School of Applied Sciences (ENSA), Ibn Tofail University, Kenitra 14000, Morocco
[2]Centre for Wireless Communications, Faculty of Information Technology and Electrical Engineering, University of Oulu, 90014 Oulu, Finland
[3]Faculty of Information Technology and Electrical Engineering, Microelectronics Research Unit, University of Oulu, 90014 Oulu, Finland
[4]Department of Electrical and Computer Engineering, Purdue University Fort Wayne, Fort Wayne, IN 46805, USA

Corresponding author: Chaïmaâ Kissi (chaimaakissi1@gmail.com)

This work was supported in part by the Academy of Finland Project 6Genesis Flagship under Grant 318927.

ABSTRACT A new antenna structure is presented in this paper. The antenna is operating at the Ultra-Wideband (UWB) band, 3.75-4.25 GHz, defined originally in Body Area Networks (BAN) part of IEEE 802.15.6 standard. The antenna size is 89 mm×60 mm×21 mm. The antenna is a directive with a measured gain of 8 dBi at 4 GHz center frequency. Since the proposed antenna is designed to meet the aspects of a receiving antenna for wireless capsule endoscopy localization, the antenna behavior in close proximity to a human body, in particular the small intestine area, is performed. For this end, initial on-body simulations were carried out by means of a tissue-layer model emulating the dielectric properties of the human body tissues at 4 GHz center frequency. This was followed by voxel model investigations. The human body impact on the antenna characteristics was analyzed firstly, followed by the examination of the power flow propagation inside the tissues. These analyses are consistent to evaluate the antenna ability to communicate with a capsule placed at the small intestine. Later, the antenna free-space propagation was assessed and validated by measurements. These results are followed by a measured on-body investigation conducted on male and female persons. Simulation results were obtained by CST Microwave Studio. Results were confirmed by measurements, conducted in an anechoic chamber at University of Oulu, Finland. The results were measured in frequency domain and later post-processed to a time domain. Consequently, measured results converge to the simulation ones. It is concluded that, the antenna could be used for Wireless Capsule Endoscopy communications with UWB signaling complying with IEEE 802.15.6 standard.

INDEX TERMS Directional radiation pattern, high gain, measurements, multi-layer model, power loss, small-intestine, UWB band, voxel model.

I. INTRODUCTION

In recent years, Ultra-Wideband (UWB) frequencies have been widely used by researchers for diverse applications [1]–[3]. UWB ranges become major field of research investigations not only for radar systems but it has been extended to Body Area Networks (BAN) applications [4]–[6], in particular, medical ones like Wireless Capsule Endoscopy [7]. Moreover, IEEE 802.15.6 standard fosters the use of UWB antennas for BAN applications [5], [8], [9]. In this context, good system relies basically on a well-designed antenna. Therefore, the accurate study of the required antenna features is one of the prime interest for both capsule and on-body antenna designs. In this regard, recently, several UWB antennas were developed to serve on-body systems for BAN applications [10]. In the literature, few papers have been dedicated to account the effect of human body on the antenna characteristics [4], [5], [11]–[13]. In [14], a significant coupling was demonstrated, by measurement, between the antenna performances and the human body tissues. The results presented in this paper are based on a pair of UWB antennas mounted on different body part of a real person, by considering different skin-antenna distances. Furthermore, many published papers are available in literature showing how the antenna characteristics affect the on-body an in-body communications [10], [15], [16]. It has also

The associate editor coordinating the review of this manuscript and approving it for publication was Shah Nawaz Burokur.

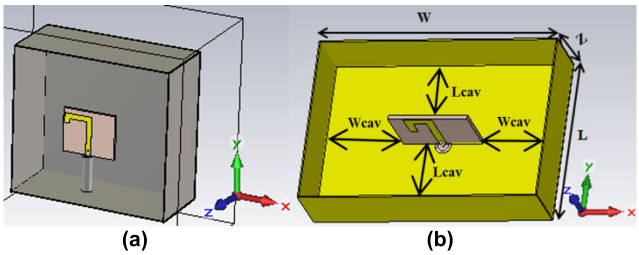

FIGURE 1. Overall view of the low-band UWB antenna in (a) "Floated" and (b) "Grounded" approaches.

been noticed that in some cases the antenna bandwidth was shifted [1] or widened [8], [9] from the referred free-space studies. Other aspects including good directivity, high gain and efficiencies are privileged for sensing, imaging, radar and medical applications [7]–[9]. To further understand the interaction of the human body with the UWB antennas, time and frequency domain analysis are required [10], [17], [18].

More recently, antenna designers have been opting for the 3.5-4.5 GHz frequency range for capsule localization purposes. This frequency selection is supported by the achievement of high image resolution and low path losses. In this direction, recent published papers were prepared by the authors to provide an extended study for wireless capsule endoscopy (WCE) communication challenges.

This paper presents an improved antenna structure of a recently presented antenna in [19], working at the mandatory channel Low-UWB band defined in IEEE 802.15.6 standard [20]. The antenna features are assessed in free-space and in close proximity to real human candidates, a female and a male, with different body shapes and weights. The measured results promote the application of the proposed antenna for BAN applications.

II. ANTENNA CONFIGURATION INVESTIGATIONS

A. ANTENNA STRUCTURE

The antenna proposed in this paper is an improvement of the structure recently and originally presented in [19], [21], and [22]. Detailed investigation of the planar antenna can be found in [22]. The requested BAN application is wireless capsule endoscopy application using the mandatory channel of Low-UWB band, ie. 3.75-4.25 GHz. Some 5G technology devices are operating at this frequency range, which my yield some interferences with capsule endoscope systems. Therefore, minimizing the antenna back radiations is one option to avoid possible interactions altering the capsule communication. At this regard, a recent published paper [21] is devoted to the study of the cavity backed ''Floated'' antenna, illustrated in Fig. 1 (a). This antenna approach is named ''Floated'' since the planar antenna itself is not connected to the reflector element. As described in [21], the ''Floated'' approach is impractical for real on-body measurements because the antenna is not rigid and the feeding point of the antenna is vulnerable to breakage. Besides that, the free-space measurement results of the ''Floated'' approach presented in [21]

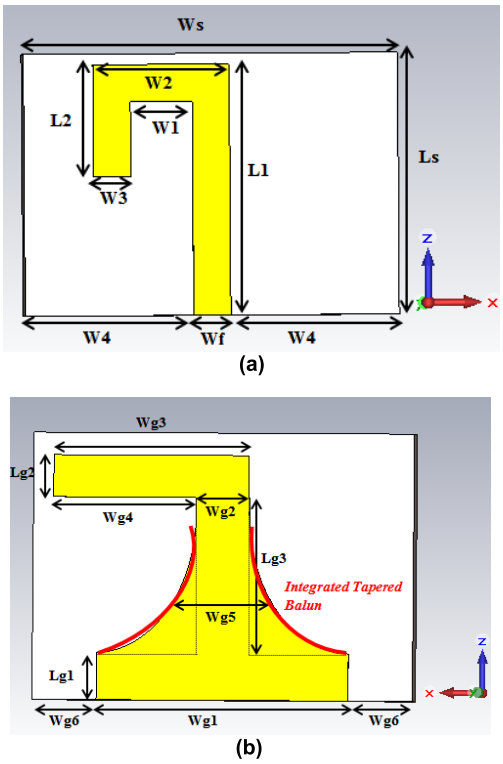

FIGURE 2. Structure of the "Grounded"UWB antenna in (a) Front and (b) Back views.

revealed some fluctuations on the radiation patterns, which are attributed to the mismatch of the antenna feeding. Hence, to remediate to the abovementioned limitations, this paper comes to briefly present the improved antenna structure and to analyze conducted on-body measurements. The proposed new antenna is named ''Grounded structure'' since the planar antenna is linked, at the feeding point, to a conductive rectangular reflector, as figured in Fig. 1 (b). Fig. 2 shows the front and back views of the simulated ''Grounded'' antenna approach. Moreover, the planar antenna is a dipole fed by a 50 Ω coaxial cable. Thus, a tapered balun [23] is required to be integrated between the unbalanced coaxial line and balanced dipole antenna, as highlighted in Fig. 2 (b), in order to cancel currents which otherwise will disturb the radio channel properties. Fig. 3 shows that the input impedance of the simulated antenna is around 50 Ω. In the rest of the paper, the studied antenna refers to the ''Grounded'' approach unless ''Floated'' approach is mentioned in the text. The antenna dimension parameters of the studied antenna structure were revised and are detailed in Table 1. The antenna overall size is 89 mm×60 mm×21 mm. The distribution of the surface current of the studied antenna, at 4 GHz, is provided in Fig. 4. A high current density is clearly seen in the edges of the radiating element, in the ground plane, as well as in the integrated tapered balun, but in the coaxial cable.

B. RESULTS ANALYSIS

The reflection coefficient of both ''Floated'' and ''Grounded'' approaches is presented in Fig. 5. The studied structure

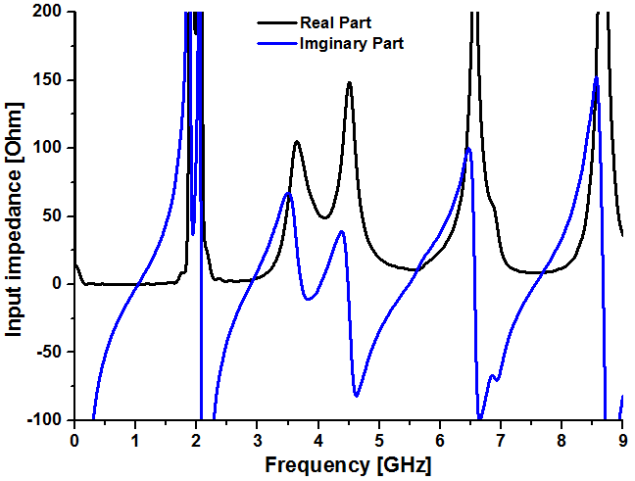

FIGURE 3. Simulated input impedance of the studied UWB antenna.

TABLE 1. Antenna parameters of the "Grounded" UWB antenna.

Parameter	Value [mm]	Parameter	Value [mm]
L	60	W4	13.6
W	89	Wg1	20
Z	21.0	Wg2	4.3
Ls	21.0	Wg3	15.5
Ws	30.2	Wg4	11.3
L1	20.14	Wg5	8.21
L2	9	Wg6	5.1
Wf	3	Lg1	3.7
W1	5	Lg2	3.3
W2	11	Lg3	12.1
W3	3		

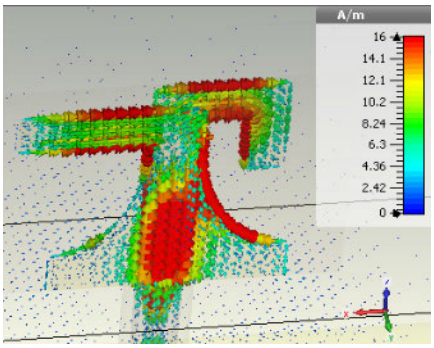

FIGURE 4. Surface current distribution at 4 GHz of the studied UWB antenna.

appears to have relatively narrower −10 dB bandwidth compared with "Floated" approach. Besides, at 4.0 GHz center frequency, the studied antenna resonates with a maximum return loss of −25 dB, while the similar value is only −15 dB for "Floated" approach. This again privileges the use of the improved studied UWB antenna. Beyond this matching investigation, the radiation pattern at 4.0 GHz was compared for both antenna approaches, as illustrated in Fig. 6. It clearly appears that the "Floated" approach achieved a directivity of 4.95 dBi towards Z-axis. However, the studied UWB antenna reached a maximum directivity of 9.84 dBi in Z-axis

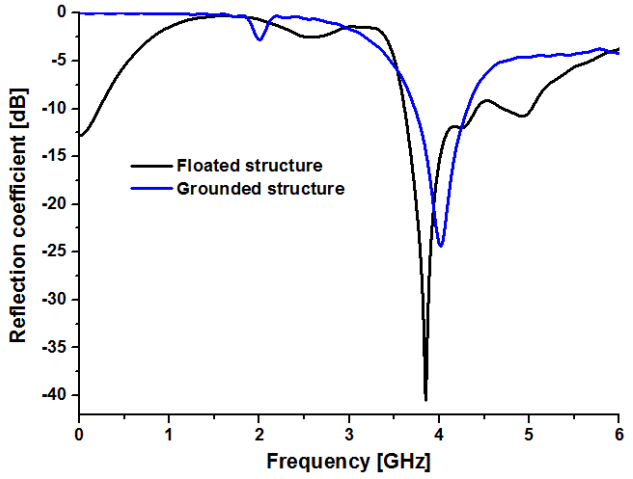

FIGURE 5. Simulated reflection coefficient of both "Floated" and "Grounded" UWB antenna structures.

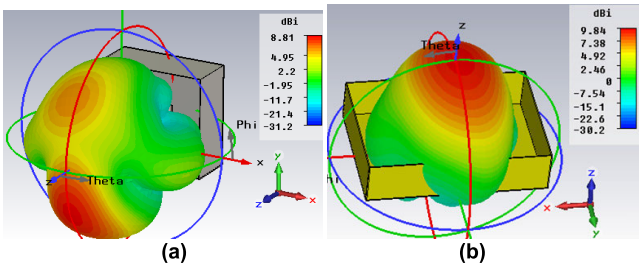

FIGURE 6. Directivity overview at 4 GHz of the (a) "Floated" and (b) "Grounded" UWB antenna structures.

direction. Knowing that the designed antenna aims to serve BAN application, the normal directivity to the body surface is of prime interest. Hence, the studied antenna approach is preferred for medical applications.

The cavity parameters *Wcav* and *Lcav* are key elements in the accurate design of the reflector. This can be seen from Fig. 7 and Fig. 8 presenting the tuning effect of *Wcav* and *Lcav*, respectively, on the antenna matching. The parameter values tested are 10 mm, 14 mm, 18.75 mm (corresponds to λ/4 at 4 GHz), 26 mm, 28 mm and 30.5 mm. According to Fig. 6, the antenna impedance matching is improved with the increase of *Wcav*. For *Wcav*=10 mm, the −10 dB bandwidth is not covered. By increasing *Wcav* up to 18.75 mm, the covered bandwidth smoothly starts to be noticed. By further decreasing *Wcav*, the covered bandwidth is significantly improved. However, the resonant frequency is softly decreased from 4.3 GHz to 4.0 GHz. Similar impedance behavior is remarked by tuning *Lcav* parameter. Better matching is achieved with *Wcav*=*Lcav*=30.5 mm. The effect of the cavity parameters tuning on the input impedance of the studied antenna is resumed in Table 2. Referring to the table, the antenna resistance dropped from 91.75 Ω to 54.34 Ω with the increase of *Wcav*. However, the resistance raised from 10.57 Ω to 54.34 Ω with the increase of *Lcav* from 10 mm to 30.5 mm. The good impedance matching is obtained for *Wcav*=*Lcav*=30.5 mm.

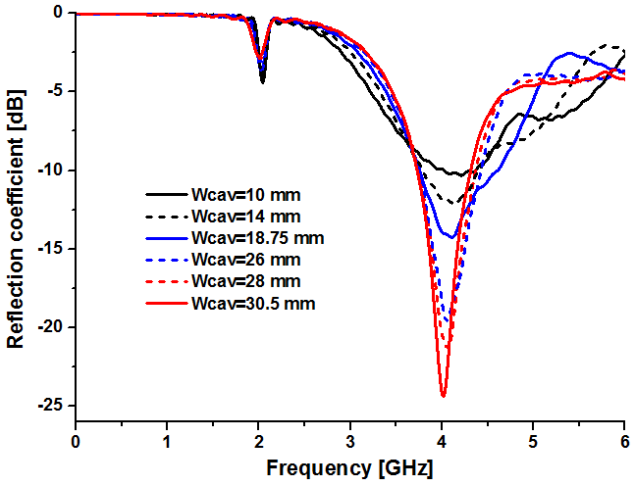

FIGURE 7. Simulated reflection coefficient of the studied UWB antenna by tuning *Wcav*.

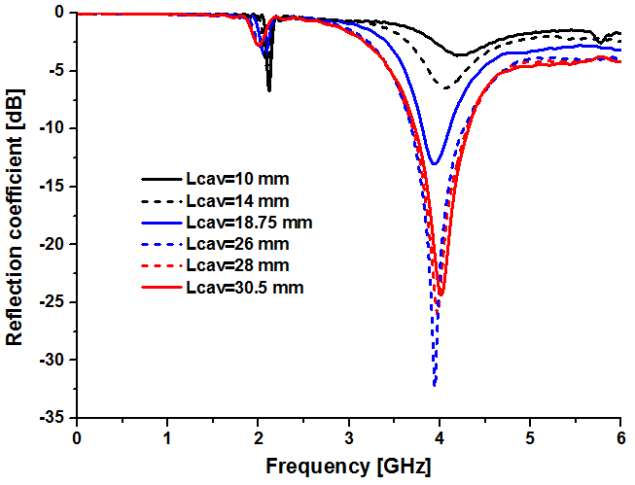

FIGURE 8. Simulated reflection coefficient of the studied UWB antenna by tuning *Lcav*.

TABLE 2. The input impedance values in Ω of the studied UWB antenna by tuning *Wcav* and *Lcav* parameters.

Parameter value	Wcav	Lcav
10 mm	91.57+j11.05	10.57-j29
14 mm	80.82+j3.90	17.16-j8.58
18.75 mm	72.29-j0.01	30.49+j7.19
26 mm	60.51-j2.43	49.70+j8.27
28 mm	58.02-j1.35	52.30+j4.75
30.5 mm	**54.34+j0.77**	**54.34+j0.77**

The studied UWB antenna is fabricated as presented in Fig. 9. The antenna characteristics, in terms of reflection coefficient and the radiation pattern, are measured in free-space with Vector Network Analyzer (VNA) and Satimo Starlab system.

Fig. 10 shows a well agreement of the simulated and measured reflection coefficient results for the studied antenna, in free-space. The studied antenna still radiates well according

FIGURE 9. Antenna prototype of the studied UWB antenna in (a) Front and (b) Back views.

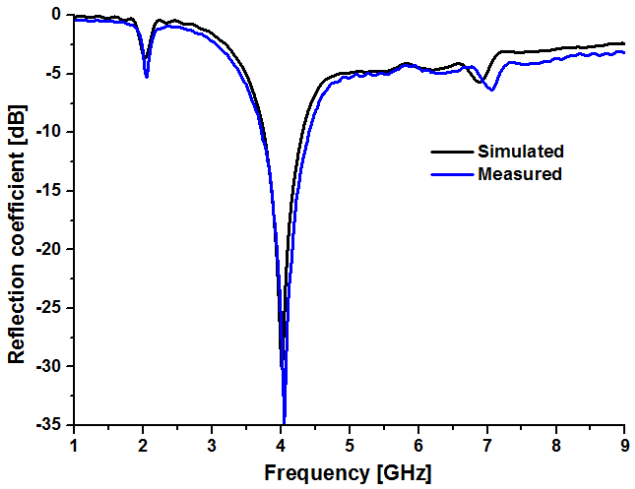

FIGURE 10. Measured vs simulated reflection coefficient of the studied antenna structure.

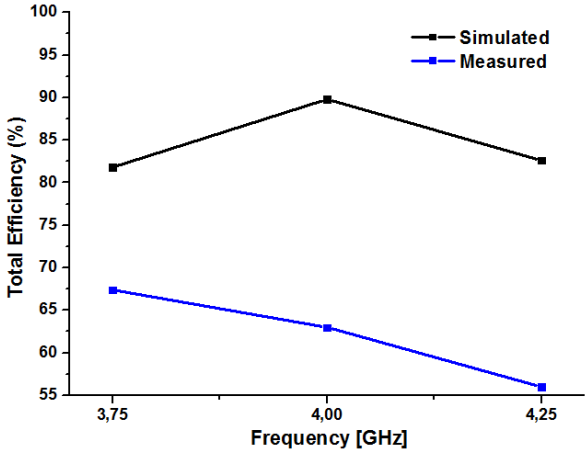

FIGURE 11. Measured total efficiency of the studied UWB antenna.

to measurement results plotted in Fig. 11, showing that 65% of the received energy is radiated by the antenna at 4 GHz. Additionally, the simulated maximum gain over the 3.75-4.25 GHz frequency band of interest is between 9 dB and 10 dB. Besides, the angular 3 dB beamwidth for constant Phi=0° is around 45° as presented in Fig. 12. This means that the studied antenna radiates equally and symmetrically to the main Z-axis direction. Hence, there is no specific orientation requirement for the antenna emplacement in practical on-body use. From Fig. 13, the measured total gain is between7.5 and 9.5 dBi over the selected frequency band of

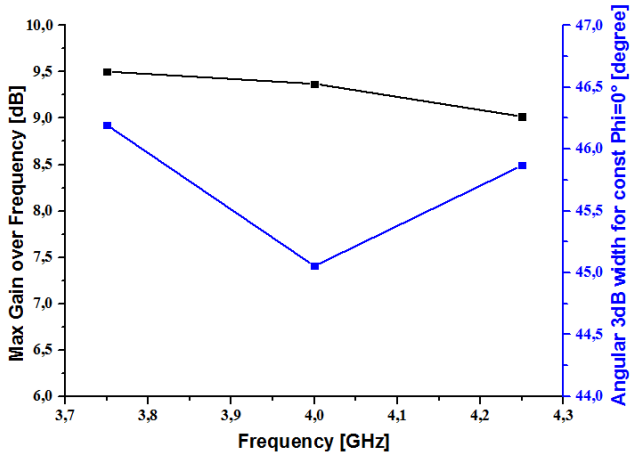

FIGURE 12. Simulated max gain over frequency and the angular 3 dB width for constant Phi=0° of the studied UWB antenna.

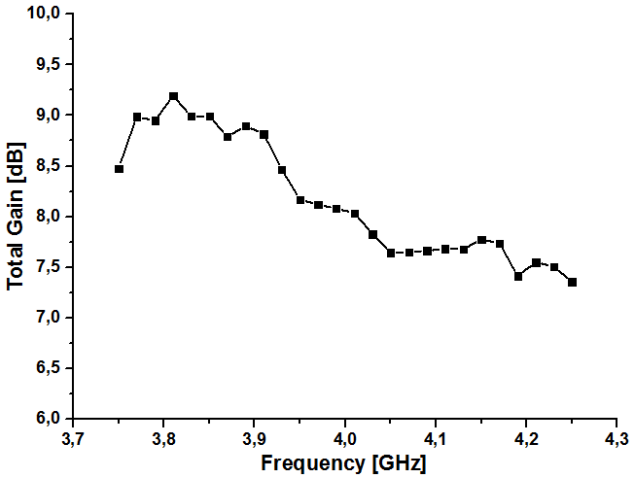

FIGURE 13. Measured gain of the studied antenna structure in free-space.

TABLE 3. Simulated and measured total gain of the studied UWB antenna.

Realized Gain – Simulated results			
Frequency [GHz]	Phi=0° [dBi]	Phi=90° [dBi]	Theta=90° [dBi]
3.75	9.04	9.03	-4.57
4	**9.39**	**9.35**	-2.81
4.25	8.73	8.73	-2.1
Total Gain – Measured results			
Frequency [GHz]	Phi=0° [dBi]	Phi=90° [dBi]	Theta=90° [dBi]
3.75	8.36	8.46	-3.93
4	**8.00**	**8.00**	-4.11
4.25	7.28	7.31	-3 .45

3.75-4.25 GHz. These measurement results validate indeed the good working of the studied antenna.

The 3D radiation pattern results of the grounded low-band UWB antenna are given in Fig. 14. Detailed measured are compared in Fig. 15 and grouped in Table 3. It is concluded that the measured gain values are 7.7 dBi, 6.8 dBi and 6.5 dBi at 3.75 GHz, 4 GHz and 4.25 GHz. Consequently, all these elements promote the good application of the studied antenna.

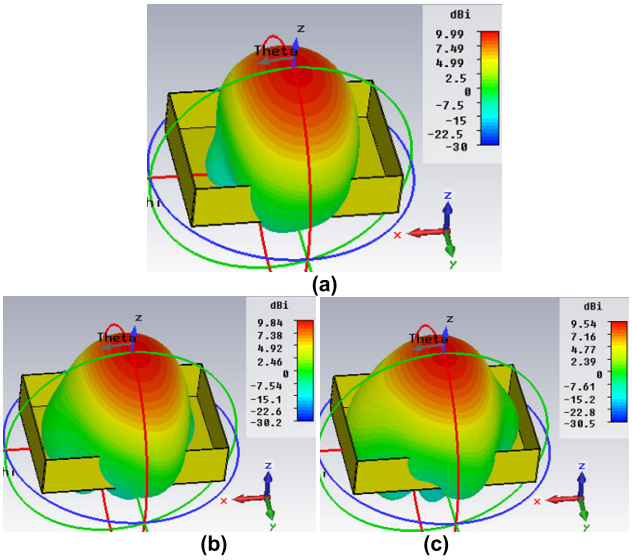

FIGURE 14. Simulated 3D Radiation pattern of the studied UWB antenna at (a) 3.75 GHz (b) 4 GHz and (c) 4.25 GHz.

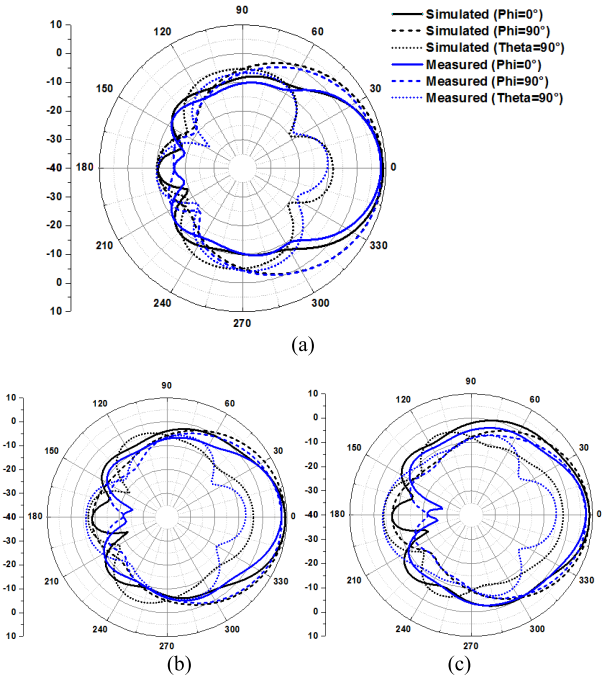

FIGURE 15. Simulated and measured radiation pattern in dBi of the studied UWB antenna in free-space at (a) 3.75 GHz, (b) 4 GHz and (c) 4.25 GHz.

III. ON-BODY INVESTIGATIONS

A. GENERAL SETUP SETTINGS

Measurements were conducted at the Centre of Wireless Communications (CWC), University of Oulu, Finland. Before starting the measurement campaign, the anechoic chamber was prepared with the required equipment settings. Since the EMC chamber was equipped with other electronic and metallic components, it was highly recommended to set a small isolated chamber inside it composed from absorber blocks. An Agilent 8720ES VNA was used to measure the

TABLE 4. Material and software settings used.

Software settings		Material settings	
Bandwidth	[1-10.6 GHz]	VNA Type	Agilent 8720ES
Sweep Time	800 ms	EMC Chamber Size	2 ×4 floor blocks (190 cm×240 cm×240 cm)
Number of sweeps	20	Cable lengths	2 cables of 8 meters length (long Sucoflex 104PEA cables)
Number of points	1601		
IF bandwidth	3 MHz		
Power	5 dBm		

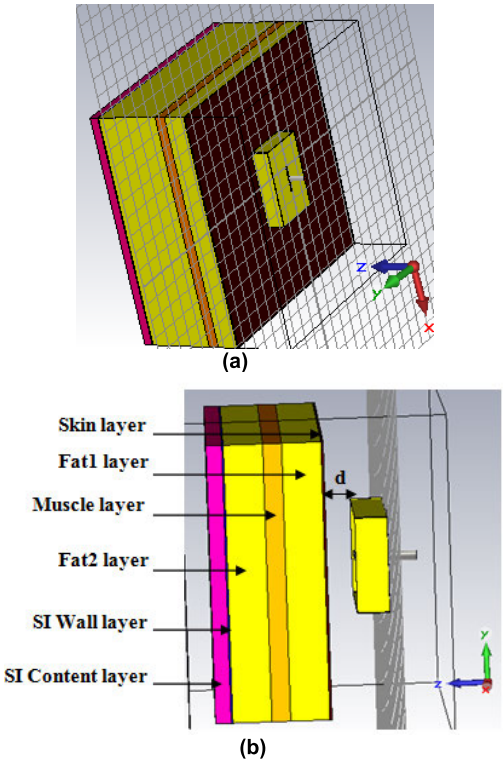

FIGURE 16. (a) Overview and (b) side view of the planar multi-layer model used.

TABLE 5. Dielectric properties of the multi-layer model at 4 GHz.

Human Tissue	Permittivity	Conductivity [S/m]	Thickness [mm]	Density [kg/m^3]
Skin Layer	2.701	40.85	1.4	1100
Fat1	0.1829	5.125	25	910
Muscle	3.015	50.82	12	1041
Fat2	0.1829	5.125	25/75	910
SI Wall	3.015	50.82	1	1020
SI Content	4.622	51.63	10	1020

reflection and transmission coefficients by using the studied antenna. Details of the measurement setup settings, in terms of materials and calibration, are provided in Table 4.

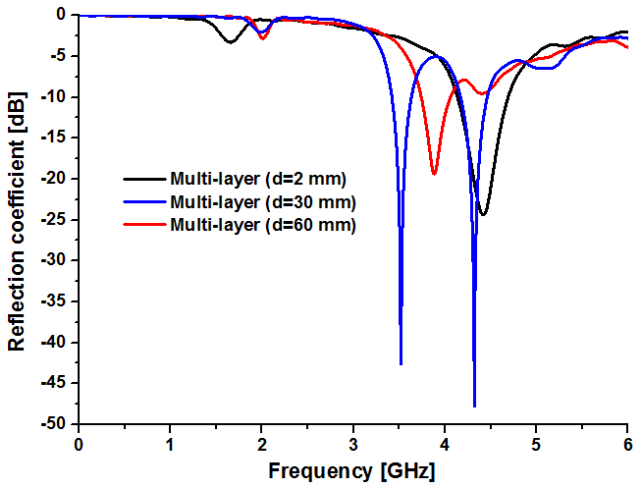

FIGURE 17. Simulated reflection coefficient of the studied UWB antenna at different distances *d* from the multi-layer model (Person A).

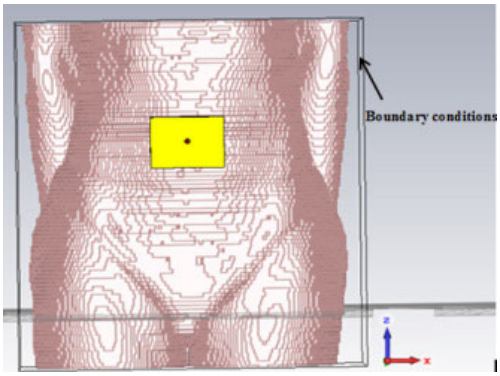

FIGURE 18. Front view of the voxel model used with the studied UWB antenna on the abdomen area.

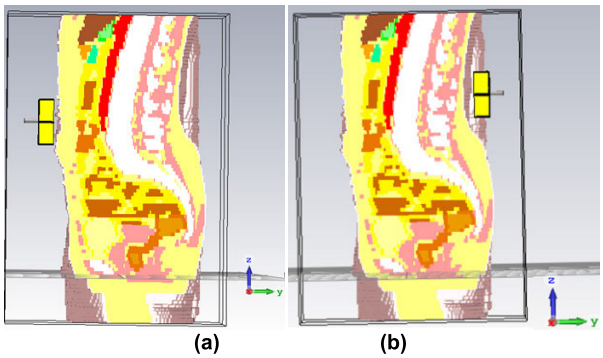

FIGURE 19. Side view of the voxel model used with the studied UWB antenna on the (a) abdomen and (b) back area.

B. ON-BODY PROPAGATION

1) SIMULATED RESULTS

The human body effect on the antenna performances is simulated in this section, by means of a planar multi-layer tissue model to emulate the dielectric properties of the human body at 4 GHz center frequency [24]–[26], as presented in Fig. 16 (a). The dielectric properties and thicknesses of the several human tissues are summarized in Table 5.

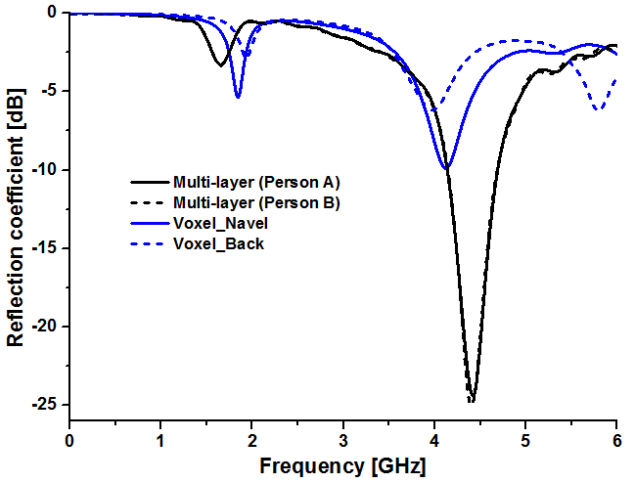

FIGURE 20. Reflection coefficient comparison of the studied UWB antenna at 2 mm distance from the human models.

The area of the multi-layer model is 280 mm×280 mm, while the height varies with the person case considered. "Person A" and "Person B" were considered to have the same tissue thicknesses, except for Fat1 layer which was chosen to be 25 mm and 75 mm, respectively. The distance d separating the cavity edge to the skin-layer is 2 mm, as marked in Fig. 16 (b). This value averages the clothes thickness. The boundary settings in the simulation model are "Open" in all directions except for Zmax it is fixed to "Open (Add space)". Fig. 17 compares the simulated reflection coefficient plots by varying the distance d. It is clearly seen how the distance strongly affects the antenna matching compared with the originally structure presented in [19]. At the closest distance of 2 mm, the −10 dB bandwidth is shifted upwards by referring to free-space. However, it is clearly noticed that the distance increase leads to a significant deterioration in the antenna matching. It seems that the studied antenna changes its behavior at different distances within the reactive near-field region. Back to theory, the boundary delimiting the near-field area of a proposed antenna is determined by the equation (1) [27].

$$R_{NF} = 0.62\sqrt{\frac{D^3}{\lambda}} \tag{1}$$

where:

R_{NF} is the boundary delimiting the reactive near-field.

D is the dimension of the smallest sphere enclosing the antenna.

λ is the wavelength at 4 GHz.

By considering dimensions of the studied antenna, it is clearly remarked from Fig. 17 that the targeted bandwidth of 3.75-4.25 GHz is obtained below −5 dB at the distances of 30 mm and 60 mm, corresponding to half and boundary of the reactive near-field. Obviously, by further raising the distance d the antenna bandwidth will converge towards free-space results. Next, on-body investigations were conducted by means of Laura2018 voxel model from CST Library, as

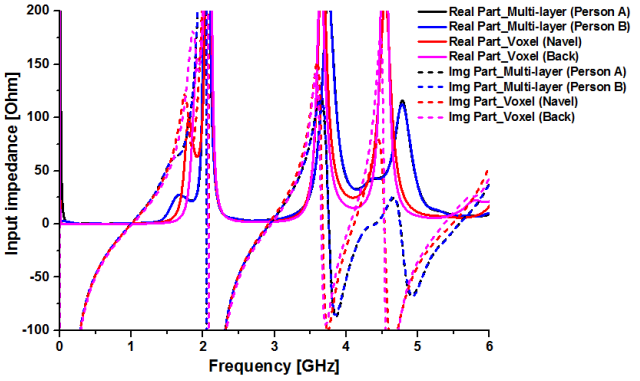

FIGURE 21. Input impedance comparison of the studied UWB antenna at 2 mm distance from the human models.

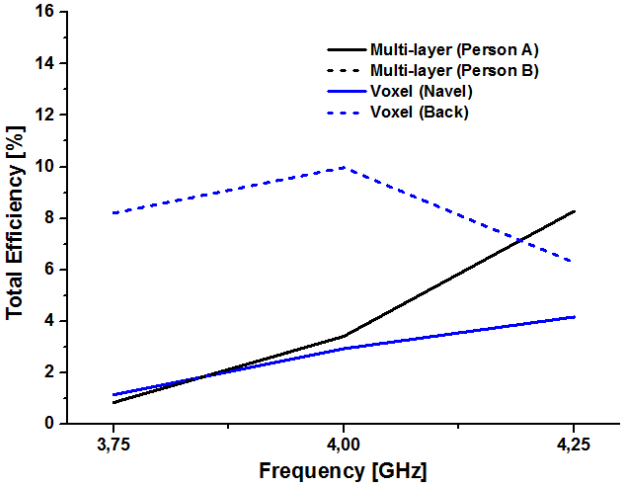

FIGURE 22. Total efficiency comparison of the studied UWB antenna at 2 mm distance from the human models.

illustrated in Fig. 18. The same boundary conditions are set with voxel model. The wearable antenna studied in this paper will act as a monitoring device for the swallowed capsule endoscope. Therefore, it is necessary to evaluate the antenna matching not only in the Abdomen Area (AA) of the body, but also in the Back Area (BA) of the human body, as shown in Fig. 19 (a) and (b), respectively. According to the results presented in Fig. 20, by considering $d = 2$ mm, the reflection coefficient of the studied antenna structure is 4.1-4.7 GHz, delimited below −10 dB, regardless the person case. However, by using the voxel model the reflection coefficient is dramatically decreased resulting in 4.10-4.43 GHz bandwidth, delimited below −5 dB, in navel position. The corresponding result is 4.03-4.13 GHz in back position. These results show how the different tissues faced by the antenna radiation have significant impact on the antenna matching. This was confirmed by measurements shown in the following section. To further analyze the reason behind this antenna-body matching, other antenna features i.e. the input impedance, the total efficiency and the 3D directivity and realized gain are provided by Fig (s). 21-26, respectively. Table 6 summarizes the reported simulation results.

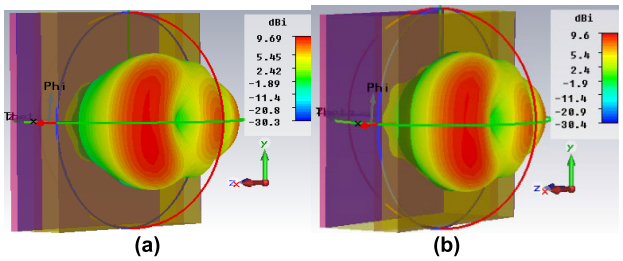

FIGURE 23. 3D directivity at 4 GHz of the studied UWB antenna at 2 mm distance from (a) Person A (b) Person B cases for the abdominal area.

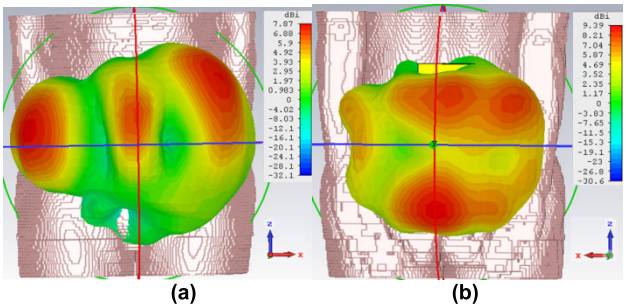

FIGURE 24. 3D directivity at 4 GHz of the studied UWB antenna at 2 mm distance from(a) Navel and (b) Back model cases.

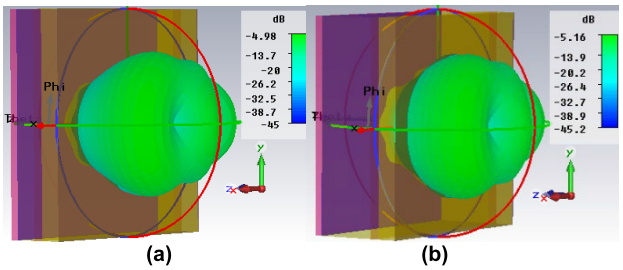

FIGURE 25. 3D gain at 4 GHz of the studied UWB antenna at 2 mm distance from (a) Person A and (b) Person B cases for the abdominal area.

The antenna resistance is 43.95 Ω, while in a corresponding realistic model known as ''Navel'' this value is 27.24 Ω. By placing the antenna on the ''Back'', the resistance drops down to 17.21 Ω. The total efficiency is around 3% using the multi-layer model and the voxel model for ''Navel'' situation. Whereas, the total efficiency is improved to 10% at the ''Back'' position. The antenna gain is about 9 dBi for Person A, Person B and the Back position against 7.87 dB for Navel case. By counting the body losses, the gain becomes in −4 - −5 dB range, except for the Back where it is of −0.62 dB. This difference is supported by the different surrounding tissues in belly and back areas.

The safety of the proposed antenna structure is evaluated by CST Microwave tool by using specific absorption rate (SAR) calculations. Maximum SAR value (10 g) is estimated of 0.103 W/kg, which is below the allowed 2 W/kg limit according to IEEE C95.3 standard [28]. The 3D SAR repartition is provided in Fig. 27.

2) MEASURED RESULTS

To further evaluate the on-body performances of the proposed grounded UWB antenna, a ''Flank-Flank'' scenario is chosen

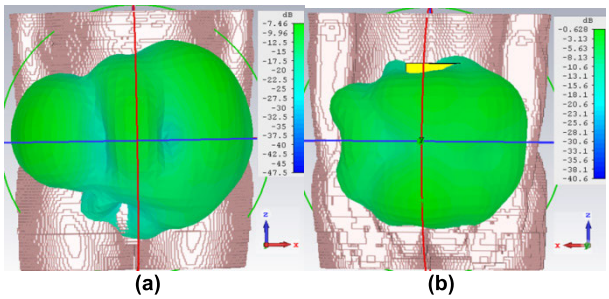

FIGURE 26. 3D gain at 4 GHz of the studied UWB antenna at 2 mm distance from (a) Navel and (b) Back model cases.

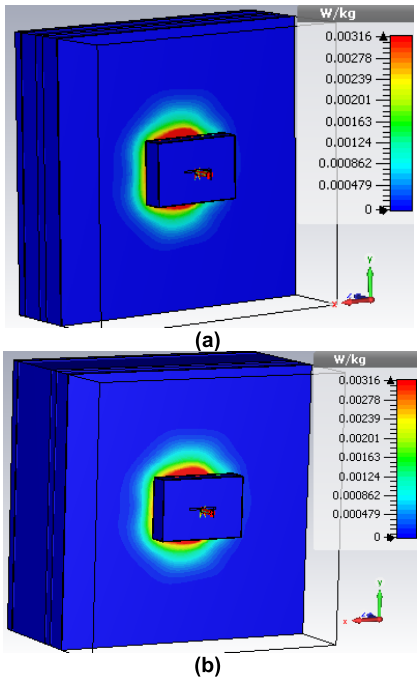

FIGURE 27. 3D SAR of the studied UWB antenna at 2 mm distance from (a) Person A and (b) Person B.

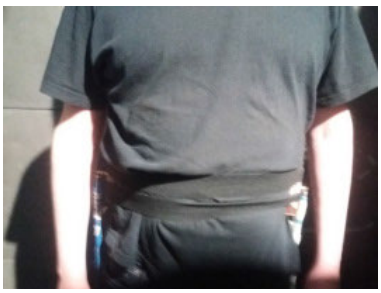

FIGURE 28. Two proposed UWB antennas placed in "Flank-Flank" position for on-body measurement scenario.

in measurements as seen in Fig. 28. This particular scenario is defined in such way that both antennas are placed at the flank of the real person. The path loss is measured in on-body scenarios for a male (M4) and female (F1) person wearing thin clothes as presented in Fig. 28. The measured path loss, over the 3.75-4.25 GHz, is in the range of −90 - −85 dB regardless the human subject, according to Fig. 29 (a). Furthermore, by analyzing the IR (Impulse Response) results in Fig. 29 (b),

TABLE 6. Input impedance, total efficiency, directivity and gain comparison at 4 GHz of the studied UWB antenna at 2mm distance from the human models.

	Person A	Person B	Navel	Back
Input impedance [Ω]	43.95-j 50.99	43.95-j 50.99	27.24-j 21.51	17.21-j 10.30
Tot Efficiency [%]	3.41	3.41	2.93	9.97
Directivity [dBi]	9.69	9.6	7.87	9.39
Gain [dB]	-4.98	-5.16	-7.46	-0.62

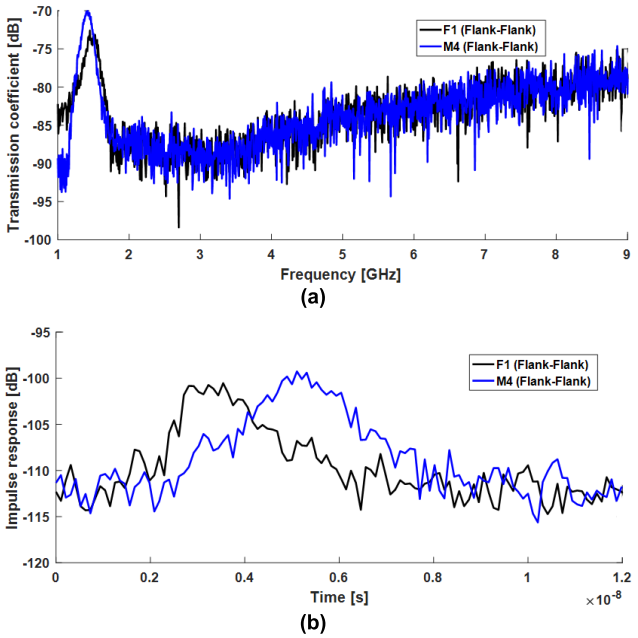

FIGURE 29. Measured (a) transmission coefficient and (c) impulse response of the studied UWB antenna on real persons in "Flank-Flank" scenario for Female (F1) and Male (M4).

one can note that the main peak occurs at 2.9 ns with a power of −100.8 dB for F1. While similarly, for the same position using the male subject, the first peak occurs at 5.1 ns with a power of −100.0 dB. Considering different antenna position on M4, it is noticed that the peak occurs at the same time with a slight increase of power around 2 dB. In addition, the body shape and size play a significant role in the on-body propagation.

The antenna impedance matching in vicinity to real human persons (F1 and M4) is given in Fig. 30 for "Flank-Flank" scenario. It is clearly seen that, the −10 dB impedance bandwidth of the proposed antenna shifted to upper frequencies in close proximity to human body compared to free-space result of 3.75-4.3 GHz. Unlike the antenna structure in [19] that shows the coverage of the bandwidth of interest of 3.75-4.25 GHz. Furthermore, the bandwidth is widened using the antenna [19]. Using the proposed antenna the covered −10 impedance bandwidth is roughly 4.1-4.7 dB and 4.0-5.1 dB for F1 and M4 persons.

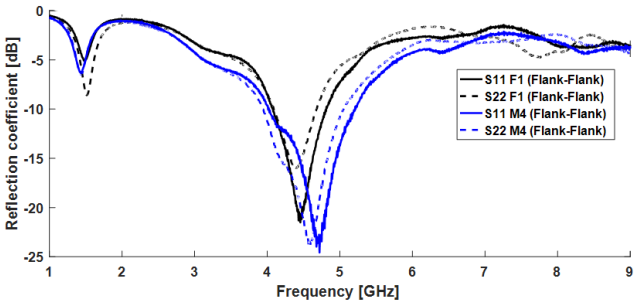

FIGURE 30. Measured transmission coefficient of the studied UWB antenna on real persons F1 and M4 for "Flank-Flank" scenario.

FIGURE 31. Two proposed UWB antennas placed on the belly area for on-body measurement scenario.

Furthermore, the antenna matching was measured for other scenarios, i.e. "AA" where two antennas are placed at the Abdomen Area, as illustrated in Fig. 31. Fig. 32 (a) shows the reflection coefficient results when two antennas are placed symmetrically to the Navel and distanced by 0 mm and 8 mm. The same bandwidth shift is noticed like in "Flank-Flank" scenario. It is clearly seen how the resonant frequency is shifted from 4 GHz (in free-space) to 4.72 GHz (in direct contact to the body by means of the thin garment). Other scenarios were assessed by placing both antennas on the back area "BA" symmetrically to a corresponding point to the Navel. The reflection coefficient was measured for different distances d of 0 mm, 5 mm and 8 mm as presented in Fig. 32 (b). As predicted previously in simulation result section, the antenna matching is deteriorated on the Back Area compared to the Abdomen Area. The paper was restricted to discuss the measured matching according to the on-body scenarios using two antennas. The allocated space of the paper does not allow the presentation in details of S12 results. Therefore, a detailed discussion based on Time and Frequency domains will be object of a following paper.

This investigation result is very important to be taken into account for the design of a coming antenna to meet the required bandwidth of 3.75-4.25 GHz, by tuning the antenna parameters accurately in close to vicinity of the body. This will be the object of an improved antenna for wireless capsule endoscopy systems.

IV. IN-BODY SIMULATION STUDY

This section is dedicated to evaluate the antenna ability for in-body communications. Since the medical application

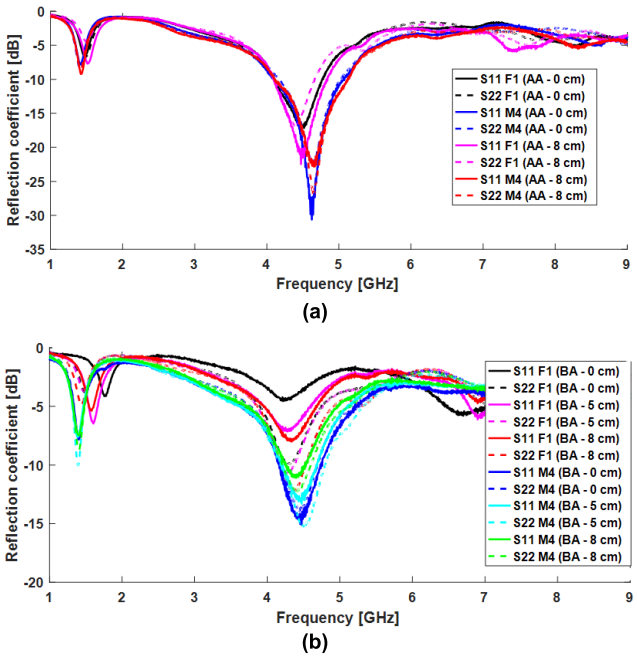

FIGURE 32. Measured transmission coefficient of the studied UWB antenna on real persons F1 and M4 for the (a) Abdomen Area "AA" and (b) Back Area "BA" scenarios.

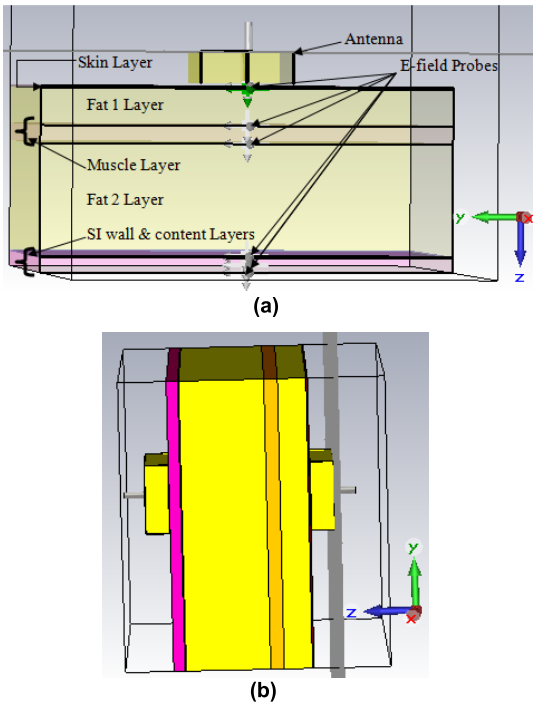

FIGURE 33. In-Body simulation of the studied UWB antenna using multi-layer model using (a) one antenna and (b) two antennas.

under investigation is Wireless Capsule Endoscopy application, the signal propagation through the body tissues is of vital importance. For this purpose, several E-field and H-field probes were situated at the interfaces presenting the difference in dielectric properties of the considered tissues faced on the abdomen area (AA). These field probes are used

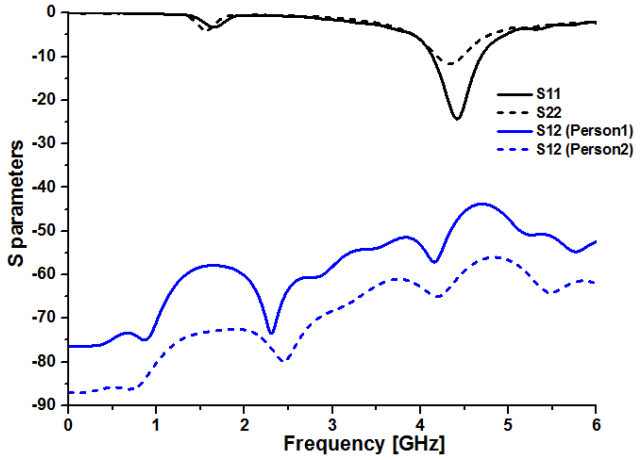

FIGURE 34. Simulated S-parameters using two proposed antennas between the multi-layer model.

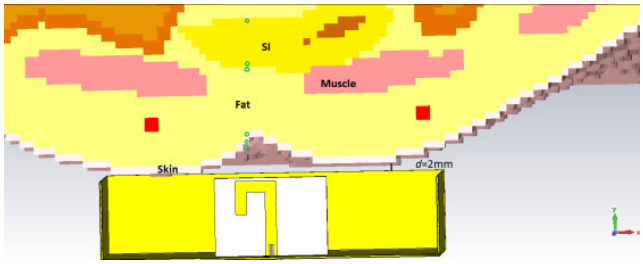

FIGURE 35. In-Body simulation of the studied UWB antenna using voxel model.

for Poynting vector (S) calculations, defined in equation (2).

$$S = \frac{1}{2} Re\left(E \times H^*\right) \tag{2}$$

$\times$ is the cross product.

$*$ is the complex conjugate.

E and H are electric and magnetic field complex values.

As described in Fig. 33 (a), the probes are positioned along a line starting from the skin layer surface (Air-Skin) to the end surface of the SI (SI-Air). Inside the tissues, the remaining probes are distributed as follows: Fat1 Surface (Skin-Fat1), Muscle Surface (Fat1-Muscle), Fat2 surface (Muscle-Fat2), SI Wall surface (Fat2-SI Wall), SI Start (SI Wall-SI Content) and SI End (SI Content-Air). The antenna was placed at 2 mm away from the multi-layer model in question. This distance represents the average thickness of a thin garment, in order to be close to realistic measurement case. Fig. 33 (b) describes the in-body simulation setup using multi-layer model.

The received power at the skin surface, using multi-layer model, is around 31 dB, as listed in Table 7. This value decreased by 2 dB at the Fat1 surface. At the muscle surface, the decline of the power is prominent about 19 dB. This value continues to decrease down to 0 dB at Fat2 surface for both cases "Person 1" and "Person 2". While at the level of the SI Wall surface, this value dropped dramatically to -20.86 dB for "Person B", and slightly to -11.61 dB for "Person A". From this result, one can conclude that 50 mm of fat tissue corresponds to 9.25 dB of power consumption.

TABLE 7. Average power at 4 GHz using multi-layer model.

Probe	Person1	Person2
Skin Interface	31.82 dB	31.75 dB
Fat1 Interface	28.99 dB	29.05 dB
Muscle Interface	10.82 dB	10.86 dB
Fat2 Interface	-0.36 dB	0.05 dB
SI Wall Interface	-11.61 dB	-20.86 dB
SI Content Interface	-12.60 dB	-21.73 dB
SI End Interface	-22.41 dB	-31.77 dB
Skin-SI Path Loss	-54.23 dB	-63.52 dB
S12 Parameter	-53.40 dB	-62.81 dB

By focusing the study on the SI content layer, it appears that this layer consumes around 10 dB. Furthermore, according to the average power results (Skin-SI Path Loss) reported in Table 7, the path loss from the skin to the end of the SI is predicted 54.23 dB and 63.52 dB for ''Person A'' and ''Person B'', respectively. Nonetheless, when placing two antennas before the skin layer and after the SI layer, the estimated path loss values based on the transmission coefficient S12 is −53.40 dB and −62.81 dB, as reported in Table 7. This good agreement in average power proves the reliability of Poynting vector and S12 parameter to predict the simulated path loss from the skin to SI tissues, which is concluded to be in 53-63 dB range. Furthermore, the reflection coefficient of the antennas depicted in Fig. 33(b) is plotted in Fig. 34. The antenna placed from the skin layer side is marked ''Antenna 1'' while the other one from the SI layer side is named ''Antenna 2''. It is clearly seen from Fig. 34 that the matching of Antenna 2 (S22) is deteriorated compared to S11. This proves how the different tissues can drastically alter the matching results. In other terms, the −10 dB bandwidth and the resonant frequency were maintained the same, while the maximum reflection coefficient was decreased from 25 dB to 12 dB. Interestingly, this result tends to the same measured matching results performed at the Back Area (BA), presented in Fig. 32 (b).

These in-body simulations are complemented by voxel model investigations. In this direction, the antenna was positioned at 2 mm from the skin surface of Laura model at the navel level. Fig. 35 illustrates the cross cut section of the voxel model with the six power probes locations marked/appearing in green circles. The first probe is located just before the skin layer. The resulting power at this position was normalized to 0 dB for easy reading. Inside the skin tissue, the reported power is −1 dB. By travelling the skin, the fat layer is faced. The power value at this layer, assumed the start of the fat layer, is −3.7 dB. By the end of the fat layer, this value decreases by 7.3 dB. By reaching the SI organ, the power achieves −13 dB at the start interface, against −25 dB at the end of the SI. Hence, the average power consumption from the skin to the SI tissues using voxel model is 25 dB. Compared to the predicted value using the multi-layer model, the voxel model-based value is far less. This is predictable since the generated signal by the antenna will find a better path to propagate within other tissues, not necessary a direct propagation path as described by the probes in Fig. 35. This in-body channel propagation challenges, using realistic voxel model, are intensively investigated in a recently published paper [29].

V. CONCLUSION AND PERSPECTIVES

A new improved antenna structure is defined in this paper. The antenna works at the Low UWB band 3.75-4.25 GHz for BAN applications, by complying with IEEE 802.15.6 standard. Its features were performed, by simulations and measurements, in the back and abdomen body parts. The antenna is proven a good candidate for Body Area Networks applications. The paper presents antenna matching close to human body. Besides a study based on frequency and time domains study comparison of the proposed grounded structure is conducted. The antenna propagation is evaluated in free-space by simulations and confirmed by measurements. These investigations were completed by on-body investigations. At this regard, different antenna dispositions were tested on the abdomen and back of the real human subjects, in particular at the navel level. Initially, simulation studies were conducted, which were followed by measurements. A well match was seen between simulation and measurement results which confirm the good operation of the antenna into interest. All aspects discussed and analyzed in the paper, promote the antenna operation for BAN applications.

ACKNOWLEDGMENT

Authors would like to thank Professor Heli Jantunen and all in Microelectronics research unit team for the help on antenna design and measurements. Anonymous reviewers are acknowledged as well for their relevant comments to improve the paper.

REFERENCES

[1] Z. N. Chen, *Antennas for Portable Devices*. Hoboken, NJ, USA: Wiley, 2007, pp. 197–217.
[2] T. Tuovinen, M. Berg, K. Y. Yazdandoost, and J. Iinatti, ''Ultra wideband loop antenna on contact with human body tissues,'' *IET Microw., Antennas Propag.*, vol. 7, no. 7, pp. 588–596, May 2013.
[3] A. S. Eltrass and N. A. Elborae, ''New design of UWB-MIMO antenna with enhanced isolation and dual-band rejection for WiMAX and WLAN systems,'' *IET Microw., Antennas Propag.*, vol. 13, no. 5, pp. 683–691, 2019.
[4] S. Wang, Y. Ji, D. Gibbins, and X. Yin, ''Impact of dynamic wideband MIMO body channel characteristics on healthcare rehabilitation of walking,'' *IEEE Antennas Wireless Propag. Lett.*, vol. 16, pp. 505–508, 2017.
[5] P. B. Samal, Z. Zakaria, and P. J. Soh, ''Compact microstrip-based textile antenna for 802.15.6 WBAN-UWB with full ground plane,'' *Int. J. Antennas Propag.*, vol. 2019, Mar. 2019, Art. no. 8283236.
[6] S. R. Zahran, M. A. Abdalla, and A. Gaafar, ''New thin wide-band bracelet-like antenna with low SAR for on-arm WBAN applications,'' *IET Microw., Antennas Propag.*, vol. 13, no. 8, pp. 1219–1225, 2019.
[7] K. M. S. Thotahewa, J.-M. Redoutè, and M. R. Yuce, ''Propagation, power absorption, and temperature analysis of UWB wireless capsule endoscopy devices operating in the human body,'' *IEEE Trans. Microw. Theory Techn.*, vol. 63, no. 11, pp. 3823–3833, Nov. 2015.
[8] D. Anzai, K. Katsu, R. Chavez-Santiago, Q. Wang, D. Plettemeier, J. Wang, and I. Balasingham, ''Experimental evaluation of implant UWB-IR transmission with living animal for body area networks,'' *IEEE Trans. Microw. Theory Techn.*, vol. 62, no. 1, pp. 183–192, Jan. 2014.

[9] H. Liu, J. Sarrazin, F. Deshours, T. Mavridis, L. Petrillo, Z. Liu, P. D. Doncker, and A. Benlarbi-Delaï, "Performance assessment of IR-UWB body area network (BAN) based on IEEE 802.15.6 standard," *IEEE Antennas Wireless Propag. Lett.*, vol. 15, pp. 1645–1648, 2016.
[10] W.-T. Shay, S.-C. Jan, and J.-H. Tarng, "A reduced-size wide slot antenna for enhancing along-body radio propagation in UWB on-body communications," *IEEE Trans. Antennas Propag.*, vol. 62, no. 3, pp. 1194–1203, Mar. 2014.
[11] W. Jeong, J. Tak, and J. Choi, "A low-profile IR-UWB antenna with ring patch for WBAN applications," *IEEE Antennas Wireless Propag. Lett.*, vol. 14, pp. 1447–1450, 2015.
[12] J.-C. Brumm and G. Bauch, "On the placement of on-body antennas for ultra wideband capsule endoscopy," *IEEE Access*, vol. 5, pp. 10141–10149, 2017.
[13] T. Otim, A. Bahillo, L. E. Díez, P. Lopez-Iturri, and F. Falcone, "FDTD and empirical exploration of human body and UWB radiation interaction on TOF ranging," *IEEE Antennas Wireless Propag. Lett.*, vol. 18, no. 6, pp. 1119–1123, Jun. 2019.
[14] W. Thompson, R. Cepeda, G. Hilton, M. A. Beach, and S. Armour, "An improved antenna mounting for ultra-wideband on-body communications and channel characterization," *IEEE Trans. Microw. Theory Techn.*, vol. 59, no. 4, pp. 1102–1108, Apr. 2011.
[15] M. Särestöniemi, C. Pomalaza-Ráez, Z. Bi, T. Kumpuniemi, C. Kissi, M. Sonkki, M. Hämäläinen, and J. Iinattit, "Comprehensive study on the impact of sternotomy wires on UWB WBAN channel characteristics on the human chest area," *IEEE Access*, vol. 7, pp. 74670–74682, 2019.
[16] P. A. Floor, R. Chávez-Santiago, A. N. Kim, K. Kansanen, T. A. Ramstad, and I. Balasingham, "Communication aspects for a measurement based UWB in-body to on-body channel," *IEEE Access*, vol. 7, pp. 29425–29440, 2019.
[17] S. Sangodoyin and A. F. Molisch, "A measurement-based model of BMI impact on UWB multi-antenna PAN and B2B channels," *IEEE Trans. Commun.*, vol. 66, no. 12, pp. 6494–6510, Dec. 2018.
[18] R. Bharadwaj, S. Swaisaenyakorn, C. G. Parini, J. C. Batchelor, and A. Alomainy, "Impulse radio ultra-wideband communications for localization and tracking of human body and limbs movement for healthcare applications," *IEEE Trans. Antennas Propag.*, vol. 65, no. 12, pp. 7298–7309, Dec. 2017.
[19] C. Kissi, M. Pomalaza-Raez, M. Särestöniemi, M. Sonkki, and M. N. Srifi, "Low-UWB directive antenna for wireless capsule endoscopy localization," presented at the BodyNets Conf., Oulu, Finland, Oct. 2018.
[20] *IEEE Standard for Local and Metropolitan Area Networks—Part 15.6: Wireless Body Area Networks*, IEEE Standard 802.15.6-2012, 2012, pp. 1–271.
[21] C. Kissi, M. Särestöniemi, T. Kumpuniemi, M. Sonkki, S. Myllymäki, M. N. Srifi, and C. Pomalaza-Raez, "On-body cavity-backed low-UWB antenna for capsule localization," *Int. J. Wireless Inf. Netw.*, pp. 1–15, 2019.
[22] C. Kissi, M. Särestöniemi, T. Kumpuniemi, M. Sonkki, S. Myllymäki, M. N. Srifi, and C. Pomalaza-Raez, "Compact directive UWB antenna for wireless capsule endoscopy localization," *Int. J. Wireless Inf. Netw.*, 2018.
[23] M. Farran, S. Boscolo, A. Locatelli, A.-D. Capobianco, M. Midrio, V. Ferrari, and D. Modotto, "Compact quasi-Yagi antenna with folded dipole fed by tapered integrated balun," *Electron. Lett.*, vol. 52, no. 10, pp. 789–790, 2016.
[24] [Online]. Available: http://www.fcc.gov/oet/rfsafety/dielectric.html
[25] [Online]. Available: https://www.itis.ethz.ch/virtual-population/tissueproperties/database/dielectric-properties/
[26] O. Akkus, A. Oguz, M. Uzunlulu, and M. Kizilgul, "Evaluation of skin and subcutaneous adipose tissue thickness for optimal insulin injection," *J. Diabetes Metabolism*, vol. 3, no. 216, p. 2, Sep. 2012.
[27] C. A. Balanis, *Antenna Theory: Analysis and Design*, 3rd ed. Hoboken, NJ, USA: Wiley, 2005, pp. 27–68.
[28] *IEEE Recommended Practice for Measurements and Computations of Radio Frequency Electromagnetic Fields With Respect to Human Exposure to Such Fields, 100 kHz-300 GHz*, IEEE Standard C95.3-2002, IEEE Standard C95.3-1991, 2003, pp. 1–126.
[29] M. Särestöniemi, C. Pomalaza-Raez, M. Berg, C. Kissi, M. Hämäläinen, and J. Iinatti, "In-body power distribution for abdominal monitoring and implant communications systems," in *Proc. ISWCS*, Oulu, Finland, Aug. 2019.

CHAÏMAÂ KISSI received the Engineering degree from the National School of Applied Sciences, Ibn Tofail University, Kenitra, Morocco, in 2015, where she is currently pursuing the Ph.D. degree with the Electronics and Telecommunication Systems Research Group, National School of Applied Sciences (ENSA), Kenitra. Her current research interest includes antenna design for medical applications.

MARIELLA SÄRESTÖNIEMI received the M.Sc. (Tech.) and Lic.Sc.(Tech.) degrees from the University of Oulu, Finland, in 2003 and 2005, respectively, where she is currently pursuing the Ph.D. degree with the Centre for Wireless Communications. Her current research interests include medical ICT, wireless body area networks, in- and on-body communications, and simulation based channel modeling and measurements.

TIMO KUMPUNIEMI received the M.Sc.(Tech.) and Lic.Sc. (Tech.) degrees from the University of Oulu, Finland, in 2001 and 2008, respectively, where he is currently pursuing the Ph.D. degree with the Centre for Wireless Communications. His current research interests include wireless medical communications, biomedical engineering, wireless body area networks, visible light communications, radio engineering on various aspects, and modulation methods. His teaching activities have been mainly on different fields of radio engineering.

MARKO SONKKI received the M.Sc. degree in electrical engineering from the Department of Electrical and Information Engineering, University of Oulu, Oulu, Finland, in 2004, and the Ph.D. degree in radio telecommunications engineering from the University of Oulu, in 2013, where he is currently a Postdoctoral Researcher with the Centre for Wireless Communications. The topic of his dissertation was wideband and multielement antennas for wireless applications focusing on antenna design based on spherical and characteristic modes theories. His current research interests include the design and analysis of wideband antennas, wideband multimode and full-duplex antennas, MIMO and diversity systems, antenna array design, and mutual coupling between antenna elements, including millimeter waves.

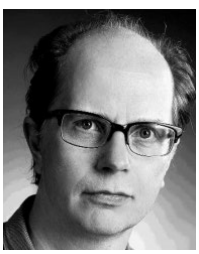

SAMI MYLLYMÄKI received the M.Sc. and D.Sc. degrees from the University of Oulu, Finland, where he is currently a Research Group Leader and an Adjunct Professor with the Microelectronics Research Unit. He has led several large industrial research projects and his teaching includes electronics packaging technology.

MOHAMED NABIL SRIFI was born in Sidi Redouane, Ouezzane, Morocco, in January 1978. He received the Licence de Physique degree in electronics from Ibn Tofail University, Kenitra, Morocco, in 1999, the Deep Higher Studies Diploma D.E.S.A. degree in telecommunications systems, and the Ph.D. degree in electrical engineering from Abdelmalek Essaâdi University, Tetuan, Morocco, in 2004 and 2009, respectively. He is currently an Assistant Professor of electrical engineering with Ibn Tofail University, Morocco. He holds two patents on antennas for ultra-wide band applications. His current research interests include biological effects of radiofrequency and microwave, bioelectromagnetics, biomedical engineering, and antenna design. He was a recipient of the National and International Awards. He is the Vice-Secretary of the Moroccan Association of Electricity, Electronics and Computers Engineering (AEECE).

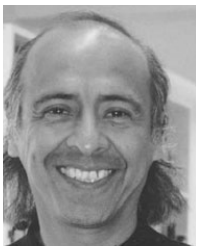

CARLOS POMALAZA-RAEZ (M'80–SM'06) received the B.S.M.E. and B.S.E.E. degrees from the Universidad Nacional de Ingeniería, Lima, Peru, in 1974, and the M.S. and Ph.D. degrees in electrical engineering from Purdue University, West Lafayette, IN, USA, in 1977 and 1980, respectively. He was a Faculty Member with the University of Limerick, Limerick, Ireland, and also with Clarkson University, Potsdam, NY, USA, and a Member of the Technical Staff with the Jet Propulsion Laboratory, California Institute of Technology, Pasadena, CA, USA. He is currently a Professor of electrical engineering with Purdue University Fort Wayne, IN, USA.